INTERNATIONAL JOURNAL FOR NUMERICAL METHODS IN FLUIDS
Int. J. Numer. Meth. Fluids 2008; **56**:845–875
Published online 4 July 2007 in Wiley InterScience (www.interscience.wiley.com). DOI: 10.1002/fld.1556

Extension of some numerical schemes to the analysis of gas and particle mixtures

J. R. García-Cascales[1,*,†], J. Mulas-Pérez[1] and H. Paillère[2]

[1]*UPCT, Departamento de Ingeniería Térmica y de Fluidos, Dr. Fleming, 30202 Cartagena, Murcia, Spain*
[2]*CEA Saclay, DM2S/SFME Laboratoire d'Etudes des Transferts et de Mécanique des Fluides, F-91191 Gif-sur-Yvette Cedex, France*

SUMMARY

In this paper, several numerical schemes are extended to obtain approximate solutions to the system of equations encountered in the analysis of multiphase mixtures of gas and particles. Both dense and dilute mixtures are studied, the gas is modelled as a perfect gas and the solid is considered incompressible. Although the tests employed throughout this work for studying the behaviour of the schemes are essentially one dimensional, the finite volume method developed permits its application to multidimensional problems in unstructured grids. Copyright © 2007 John Wiley & Sons, Ltd.

Received 4 July 2006; Revised 5 April 2007; Accepted 22 May 2007

KEY WORDS: numerical methods; multiphase mixtures; dusty flow; two-phase flow

1. INTRODUCTION

Solid particles and gas mixtures are encountered in many industrial applications such as fluid catalytic crackers, fluidized bed combustors, ventilation systems and so forth. In certain fields—for example, agricultural, chemical, metallurgical or nuclear industry—special interest has been paid to these mixtures because of safety reasons. Problems related to dust mobilization or dust combustion have become fundamental issues due to the existing risks for population and for other nearby facilities.

In nuclear fusion, the amount of dust inside a tokamak as the ITER is limited due to the problems which may cause in the plasma and second because a loss of vacuum or an air ingress accident could cause that radioactive products abandon the vacuum vessel and contaminate the surrounding area. Even in the case that a loss of coolant took place, hydrogen might be generated

*Correspondence to: J. R. García-Cascales, UPCT, Departamento de Ingeniería Térmica y de Fluidos, Dr. Fleming, 30202 Cartagena, Murcia, Spain.
†E-mail: jr.garcia@upct.es

or a dust deflagration or detonation might occur. The objective of this work is to contribute to the development of a reliable tool for analysing dust mobilizing problems. In general, the type of mixture expected to be encountered inside the vacuum vessel of a fusion reactor is polydispersed and belongs to the high-dilute mixtures although, here, dense mixture models have also been considered in order to study the cases in which particle–particle interaction is also important.

The way of modelling these problems depends on several factors such as the application considered, the type of particles and their size, the interaction between the phases and the internal reactions or the problem geometry. The sort of problem faced in each case determines which model is chosen. As such, great efforts have been made in order to find proper physical models capable of characterizing each particular dust and gas mixture and, also, of developing suitable numerical schemes for the solution of the resulting systems of equations. With regards to the physical models, Gidaspow's model, [1] and its subsequent reviews stand out from other models. In the detonation-to-deflagration of dusty gas the Baer–Nunziato model [2] and its recent reviews [3] are applicable.

Throughout this work, some numerical schemes for the analysis of dust and gas mixtures are proposed. In particular, AUSM$^+$up and Rusanov schemes have been extended depending on the case. As the other members of the AUSM family of schemes, the AUSM$^+$up scheme has some characteristics which make it quite an appealing scheme [4]:

- They do not require any characteristic analysis or field-by-field decomposition.
- They have the ability to capture steady contact discontinuities exactly.
- They have the capability of being easily adaptable to different flow models such as compressible and near incompressible flows.
- They require less CPU than most Godunov-type solvers per flux evaluation.

In their application, this paper takes advantage of the simplifications that the different approaches allow. It has been organized as follows. Firstly, the general system of equations for dust and gas mixtures is presented. Then, the assumptions adopted throughout this paper and the systems of equations for each level of approximation studied are described: i.e. dense, dilute and high-dilute mixtures. The mathematical nature of the aforementioned systems and some possible numerical schemes, most of which are extensions of the AUSM$^+$up scheme [5], are introduced to solve them. Finally, the behaviour of these schemes is tested with some numerical problems. Following this, some conclusions are drawn.

2. SYSTEM OF EQUATIONS

The system of equations which characterizes a two-phase mixture of particles and gas in the Baer–Nunziato model is given by a set of three balance equations for mass, momentum and energy of each phase. This is completed by a seventh equation which accounts for the particle compaction which provides the time evolution of the particle volume fraction. This model considers two different pressures for the phases and is given by

$$\frac{\partial \alpha_g \rho_g}{\partial t} + \nabla \cdot (\alpha_g \rho_g \mathbf{u}_g) = \Gamma_g$$

$$\frac{\partial \alpha_g \rho_g u_g}{\partial t} + \nabla \cdot (\alpha_g \rho_g \mathbf{u}_g \otimes \mathbf{u}_g + \alpha_g p_g \bar{I}) = p_g \nabla \alpha_g + \mathbf{F}_{dg} + \Phi_{mg}$$

DOI: 10.1002/fld

$$\frac{\partial \alpha_g \rho_g E_g}{\partial t} + \nabla \cdot (\alpha_g \rho_g \mathbf{u}_g H_g + \alpha_g p_g \bar{I}) = -p_g \frac{\partial \alpha_g}{\partial t} + \mathbf{F}_{dg} \cdot \mathbf{u}_p + Q_g + \Phi_{eg}$$

$$\frac{\partial \alpha_p \rho_p}{\partial t} + \nabla \cdot (\alpha_p \rho_p \mathbf{u}_p) = -\Gamma_g \tag{1}$$

$$\frac{\partial \alpha_p \rho_p u_p}{\partial t} + \nabla \cdot (\alpha_p \rho_p \mathbf{u}_p \otimes \mathbf{u}_p + \alpha_p p_p \bar{I}) = p_p \nabla \alpha_p - \mathbf{F}_{dg} + \Phi_{mp}$$

$$\frac{\partial \alpha_p \rho_p E_p}{\partial t} + \nabla \cdot (\alpha_p \rho_p \mathbf{u}_p H_p + \alpha_p p_p \bar{I}) = -p_p \frac{\partial \alpha_p}{\partial t} - \mathbf{F}_{dg} \cdot \mathbf{u}_p - Q_g + \Phi_{ep}$$

$$\frac{\partial \alpha_p}{\partial t} + \mathbf{u}_p \cdot \nabla \alpha_p = \frac{\alpha_g \alpha_p}{\mu_c}[p_p - p_g - \beta_p] + \frac{\Gamma_g}{\rho_p}$$

where e_k is the phase specific internal energy, E_k the total internal energy of phase k, $E_k = e_k + |\mathbf{u}_k|^2/2$, F_{dk} the drag force, h_k the specific enthalpy, H_k the total enthalpy of phase k, $H_k = h_k + |\mathbf{u}_k|^2/2$, p_k the pressure, Q the interfacial convective heat transfer, t the time, u_k the velocity, α_k the phase volume fraction ($\alpha_g + \alpha_p = 1$), β_k the configuration pressure and Φ_m and Φ_e the other momentum and energy source terms, respectively. They account for interfacial exchanges of momentum and energy, other external forces interactions (shear stress, Reynolds stress and so on), internal energy generation and so forth.

In Equation (1), Γ_g is the interfacial mass exchange due to phase change, chemical reactions, etc., μ_c the dynamic compaction viscosity and ρ_k the phase density.

Subscripts and superscripts: k is a general phase, g the gas phase and p the solid or particle phase.

Particle–particle interaction is negligible in dilute gas–particle flows. It is only when the particle concentration becomes higher that the particles collide with each other and lose kinetic energy. In dense flows, the force on the particles due to shear stress in the continuum phase is traditionally neglected and a term is added to the particle momentum equation characterizing the particle–particle interaction [6], this is

$$\frac{\partial \alpha_p \rho_p u_p}{\partial t} + \nabla \cdot (\alpha_p \rho_p \mathbf{u}_p \otimes \mathbf{u}_p + \alpha_p p_p \bar{I}) = p_p \nabla \alpha_p - G \nabla \alpha_p - \mathbf{F}_{dg} + \Phi_{mp} \tag{2}$$

where G is the solid stress modulus which characterizes this effect and is obtained from empirical correlations. Different approaches can be found in the existing literature, Tsuo and Gidaspow who used this model for the study of circulating beds [7], and Harris and Crighton who proposed a simple model for the stress modulus [8]:

$$G = P_s \frac{\alpha_{p,0}}{\alpha_{p,0} - \alpha_p} \tag{3}$$

where $\alpha_{p,0}$ the maximum solid volume fraction. Similar approaches can be found in Combe and Hérard [9], Krispin and Collins [10], Toro [11], Rogue *et al.* [12], and Saurel *et al.* [13]. Instead of adding this term, some authors include this effect in the solid pressure by means of a stress

DOI: 10.1002/fld

tensor in such a way that

$$p_p = p_g + \tilde{T} \tag{4}$$

where $\tilde{T}$ is a stress tensor which represents the particle–particle interaction.

When a high-dilute mixture is considered, System (1) can be simplified, assuming:

- Particle volume fraction can be neglected against gas volume fraction, so in the gas system of equations $\alpha_g \simeq 1$ is assumed.
- Pressure effect is negligible in the particle phase so pressure disappears from the particle system of equations, whereas both systems remain coupled only by the source terms.
- Solid phase is considered incompressible and its system of equations is written in terms of the particle concentration $\sigma = \alpha_p \rho_p$.

In what follows, particles are assumed to be spherical and only gravitational force, interfacial friction and convective heat transfer between the phases are included in the model. Thus, the system of equations (1) is reduced to

$$\begin{gathered}
\frac{\partial \rho_g}{\partial t} + \nabla \cdot (\rho_g \mathbf{u}_g) = 0 \\
\frac{\partial}{\partial t}(\rho_g \mathbf{u}_g) + \nabla \cdot (\rho_g \mathbf{u}_g \otimes \mathbf{u}_g + p) = \rho_g \mathbf{g} + \mathbf{F}_{dg} \\
\frac{\partial}{\partial t}(\rho_g E_g) + \nabla \cdot (\rho_g \mathbf{u}_g H_g) = \rho_g \mathbf{u}_g \cdot \mathbf{g} + \mathbf{F}_{dg} \cdot \mathbf{u}_p + Q_g \\
\frac{\partial \sigma}{\partial t} + \nabla \cdot (\sigma \mathbf{u}_p) = 0 \\
\frac{\partial}{\partial t}(\sigma \mathbf{u}_p) + \nabla(\sigma \mathbf{u}_p \otimes \mathbf{u}_p) = \sigma \mathbf{g} - \mathbf{F}_{dg} \\
\frac{\partial}{\partial t}(\sigma E_p) + \nabla \cdot (\sigma \mathbf{u}_p E_p) = \sigma \mathbf{u}_p \cdot \mathbf{g} - \mathbf{F}_{dg} \cdot \mathbf{u}_p - Q_g
\end{gathered} \tag{5}$$

where $\mathbf{g}$ is the gravity vector, E_p is the total internal energy of the particle, given by $E_p = c_m T_p + |\mathbf{u}_p|^2/2$, and c_m is the particle specific heat at constant volume. The closure relationships are defined in the following sections depending on the test. A direct consequence of these simplifications is the modification of the mathematical structure of System (1) as the sub-system corresponding to the particles is degenerate hyperbolic (system of equations (5)).

In all the tests studied below, the gas phase is modelled as a perfect gas:

$$\rho_g = \frac{p}{(\gamma_g - 1) e_g} \tag{6}$$

where γ_g is the specific heat ratio of the gas phase. However, when the flow is considered isentropic, it is modelled by means of the following equation:

$$\rho_g = \left(\frac{p}{\kappa}\right)^{1/\gamma_g} \tag{7}$$

where κ has pressure units.

DOI: 10.1002/fld

Other approximations of System (1) may be found in the existing literature, many of them include turbulence models, reactions, collisions, coalescence and other interactions whose consideration is beyond the scope of this model.

3. NUMERICAL SCHEMES

In this section, the extension of some numerical schemes is studied. The finite volume method employed is briefly described and several schemes are proposed to solve the different approximations of the problems introduced. A second-order version based on variable extrapolations is also suggested.

3.1. Finite volume method

The system of equations (5) may be written in vector form as

$$U_t + \nabla \cdot \mathscr{H}(U) = S(U) \tag{8}$$

where U is the conserved variable vector and $\mathscr{H} = [F\ G\ H]$ the flux tensor. The integration of the homogeneous part of this system in a control volume Ω yields

$$\frac{\mathrm{d}}{\mathrm{d}t} \iiint_{\Omega} U \,\mathrm{d}\Omega + \iint_{A} \mathscr{H} \cdot \hat{n} \,\mathrm{d}A = 0 \tag{9}$$

where A is the boundary of Ω and $\hat{n}$ is the normal vector to surface A. Taking the first integral as a time rate of change of the average of the conserved variables U in each control volume and considering the boundary A formed by N surfaces in such a way that $A = \bigcup_{s=1}^{N} A_s$, Equation (9) can be written as

$$\frac{\mathrm{d}U}{\mathrm{d}t} + \frac{1}{|\Omega|} \sum_{s=1}^{N} \iint_{A_s} \mathscr{H} \cdot \hat{n} \,\mathrm{d}A = 0 \tag{10}$$

By discretizing the time derivative and by approaching the surface integral of the flux by $\iint_{A_s} \mathscr{H} \cdot \hat{n} \,\mathrm{d}A \simeq T_s^{-1} F(T_s U) A_s$, a finite volume scheme for multiple dimensions in unstructured grids is obtained, such that

$$U_j^{n+1} = U_j^n - \frac{\Delta t}{|\Omega|} \sum_{s=1}^{N} T_s^{-1} F(T_s U) A_s \tag{11}$$

where A_s is the area of the sth surface which bounds volume Ω, T_s is the rotation matrix and T_s^{-1} its inverse.

A common practice is to solve the system of equations by using splitting schemes. Firstly, the following PDE is solved by means of the above finite volume approach:

$$U_t + \nabla \cdot F(U) = 0 \tag{12}$$

with the initial conditions $U(x, t^n) = U^n$, and its solution is then used as an initial condition of the ODE problem:

$$\frac{\mathrm{d}}{\mathrm{d}t} U = S(U) \tag{13}$$

DOI: 10.1002/fld

which is usually solved by using a Runge–Kutta method, an explicit or implicit Euler method or any other available method. A first-order scheme is obtained if the system of Equation (12) is solved as follows:

$$U_j^n = \mathscr{L}_s^{\Delta t}\,\mathscr{L}_h^{\Delta t} U_i^n \tag{14}$$

where $\mathscr{L}_s^{\Delta t}$ stands for the integration operator for the source term and $\mathscr{L}_h^{\Delta t} U_i^n$ stands for the advection operator. In order to have a second-order scheme, previous operators are applied as

$$U_j^n = \mathscr{L}_s^{\Delta t/2}\,\mathscr{L}_h^{\Delta t}\,\mathscr{L}_s^{\Delta t/2} U_i^n \tag{15}$$

In this development, explicit unsplit schemes are used, approximating solutions at time $n+1$ for the different models by means of

$$U_j^{n+1} = U_j^n - \frac{\Delta t}{|\Omega|}\sum_{s=1}^{N} T_s^{-1} F(T_s U) A_s + \Delta t\, S^n(U^n) \tag{16}$$

3.2. Numerical scheme

In what follows, different schemes are suggested for the models considered along this work, heavy-laden, dilute and high-dilute mixtures.

3.2.1. Heavy-laden mixtures. In this case, the interaction between particles is important and it is modelled by means of a pressure interaction term. The AUSM$^+$up scheme [5] has been applied to estimate the numerical flux corresponding to this type of mixtures of gas and particles. This numerical method is quite robust and works quite well at any speed. With this extension, some spurious oscillations encountered at certain discontinuities with other numerical schemes are avoided. The conserved variable vector and the flux vectors are given by

$$U = \begin{bmatrix} \alpha\rho_g \\ \alpha\rho_g u_{gx} \\ \alpha\rho_g u_{gy} \\ \alpha\rho_g u_{gz} \\ \alpha\rho_g E_g \\ (1-\alpha)\rho_p \\ (1-\alpha)\rho_p u_{px} \\ (1-\alpha)\rho_p u_{py} \\ (1-\alpha)\rho_p u_{pz} \\ (1-\alpha)\rho_p E_p \end{bmatrix}, \quad F = \begin{bmatrix} \alpha\rho_g u_{gx} \\ \alpha\rho_g (u_{gx}^2 + p_g) \\ \alpha\rho_g u_{gx} u_{gy} \\ \alpha\rho_g u_{gx} u_{gz} \\ \alpha\rho_g u_{gx} H_g \\ (1-\alpha)\rho_p u_{px} \\ (1-\alpha)\rho_p (u_{px}^2 + p_p) \\ (1-\alpha)\rho_p u_{px} u_{py} \\ (1-\alpha)\rho_p u_{px} u_{pz} \\ (1-\alpha)\rho_p u_{px} (E_p + p_p/\rho_p) \end{bmatrix} \tag{17}$$

DOI: 10.1002/fld

$$G=\begin{bmatrix}\alpha\rho_g u_{gy}\\ \alpha\rho_g u_{gy}u_{gx}\\ \alpha\rho_g(u_{gy}^2+p_g)\\ \alpha\rho_g u_{gy}u_{gz}\\ \alpha\rho_g u_{gy}H_g\\ (1-\alpha)\rho_p u_{py}\\ (1-\alpha)\rho_p u_{py}u_{px}\\ (1-\alpha)\rho_p(u_{py}^2+p_p)\\ (1-\alpha)\rho_p u_{py}u_{pz}\\ (1-\alpha)\rho_p u_{py}(E_p+p_p/\rho_p)\end{bmatrix},\quad H=\begin{bmatrix}\alpha\rho_g u_{gz}\\ \alpha\rho_g u_{gz}u_{gx}\\ \alpha\rho_g u_{gz}u_{gy}\\ \alpha\rho_g(u_{gz}^2+p_g)\\ \alpha\rho_g u_{gz}H_g\\ (1-\alpha)\rho_p u_{pz}\\ (1-\alpha)\rho_p u_{pz}u_{px}\\ (1-\alpha)\rho_p u_{pz}u_{py}\\ (1-\alpha)\rho_p(u_{pz}^2+p_p)\\ (1-\alpha)\rho_p u_{pz}(E_p+p_p/\rho_p)\end{bmatrix} \tag{18}$$

In this approximation, S is the source term which groups, the non-conservative terms, the gravitational effects, the interfacial friction, and the interfacial heat transfer. Thus,

$$S=\begin{bmatrix}0\\ p_g\dfrac{\partial\alpha}{\partial x}+\alpha g_x+F_{dx}\\ p_g\dfrac{\partial\alpha}{\partial y}+\alpha g_y+F_{dy}\\ p_g\dfrac{\partial\alpha}{\partial z}+\alpha g_z+F_{dz}\\ \alpha\mathbf{u}_g\cdot\mathbf{g}+\mathbf{F}_d\cdot\mathbf{u}_p+Q_g\\ 0\\ -p_g\dfrac{\partial\alpha}{\partial x}+(1-\alpha)g_x-F_{dx}\\ -p_g\dfrac{\partial\alpha}{\partial y}+(1-\alpha)g_y-F_{dy}\\ -p_g\dfrac{\partial\alpha}{\partial z}+(1-\alpha)g_z-F_{dz}\\ (1-\alpha)\mathbf{u}_p\cdot\mathbf{g}-\mathbf{F}_d\cdot\mathbf{u}_p-Q_g\end{bmatrix} \tag{19}$$

Following the AUSM family of schemes [5, 14, 15], the flux vector is split into a convective part and a pressure part, such that for the phase k

$$F_k=F_k^{(c)}+F_k^{(p)}$$

DOI: 10.1002/fld

where $F_k^{(c)} = \dot{m}_k \Psi_k$, with the mass flow rate given by $\dot{m}_k = \rho_k M_k c_k$. $M_k = u_{kn}/c_k$ is the mach number, c_k is the speed of sound, and

$$\Psi_k = \begin{pmatrix} 1 \\ u_{kn} \\ u_{kt_1} \\ u_{kt_2} \\ H_k \end{pmatrix} \quad \text{and} \quad F_k^{(p)} = \begin{pmatrix} 0 \\ \alpha_k p_k \\ 0 \\ 0 \\ 0 \end{pmatrix}$$

where p_k includes intergranular effects in the particle case. n, t_1 and t_2, respectively, refer to the normal and tangential directions in the local reference frame. Dropping the subscript k from the equations, the numerical flux can be written as

$$F_{1/2} = F_{1/2}^{(c)} + F_{1/2}^{(p)}$$

with $F_{1/2}^{(c)}$ is the numerical convective flux through the interface s and $F_{1/2}^{(p)}$ the numerical pressure flux through the interface s.

For phase k, the numerical convective flux at the interface $1/2$ is given by

$$F_{1/2}^{(c)} = \dot{m}_{1/2}(u_{\mathrm{L}}, u_{\mathrm{R}}) \psi_{1/2}(u_{\mathrm{L}}, u_{\mathrm{R}})$$

where the left and right states are denoted by L (left) and R (right)

$$\psi_{1/2}(u_{\mathrm{L}}, u_{\mathrm{R}}) = \begin{cases} \Psi_{\mathrm{L}} & \text{if } \dot{m}_{1/2} \geqslant 0 \\ \Psi_{\mathrm{R}} & \text{otherwise} \end{cases}$$

The pressure flux is simply given by

$$F_{1/2}^{(p)} = (0,\, p_{1/2}(u_{\mathrm{L}}, u_{\mathrm{R}}),\, 0,\, 0,\, 0)^t$$

In this extension of the AUSM$^+$up scheme, the interface variables $\dot{m}_{1/2}$ and $p_{1/2}$ are defined for the gas phase as

$$\dot{m}_{g,1/2} = c_{g1/2} M_{g1/2} \begin{cases} \alpha_{\mathrm{L}} \rho_{g\mathrm{L}} & \text{if } M_{g1/2} > 0 \\ \alpha_{\mathrm{R}} \rho_{g\mathrm{R}} & \text{otherwise} \end{cases} \tag{20}$$

and for the particles as

$$\dot{m}_{p,1/2} = c_{1/2} M_{1/2} \rho_p \begin{cases} (1 - \alpha_{\mathrm{L}}) & \text{if } M_{p1/2} > 0 \\ (1 - \alpha_{\mathrm{R}}) & \text{otherwise} \end{cases} \tag{21}$$

where $M_{k1/2}$ is based on polynomial functions of the Mach numbers (M_k) of left and right states. Dropping the subscript k

$$M_{1/2} = \mathscr{M}_{(4)}^{+}(M_{\mathrm{L}}) + \mathscr{M}_{(4)}^{-}(M_{\mathrm{R}}) - \frac{K_p}{f_a} \max(1 - \sigma \tilde{M}^2, 0) \frac{p_{\mathrm{R}} - p_{\mathrm{L}}}{p_{\mathrm{R}} + p_{\mathrm{L}}} \tag{22}$$

DOI: 10.1002/fld

where $0 \leqslant K_p \leqslant 1$ and $\sigma \leqslant 1$,

$$\tilde{M}^2 = \frac{(u_{\mathrm{L}}^2 + u_{\mathrm{R}}^2)}{2} c_{1/2}^2$$

$$M_o^2 = \min(1, \max(\tilde{M}^2, M_\infty^2)) \in [0, 1]$$

$$f_a(M_o) = M_o(2 - M_o) \in [0, 1]$$

$$\begin{aligned} p_{1/2} = {} & \mathscr{P}_{(5)}^{+}(M_{\mathrm{L}})\alpha_{\mathrm{L}} p_{\mathrm{L}} + \mathscr{P}_{(5)}^{-}(M_{\mathrm{R}})\alpha_{\mathrm{R}} p_{\mathrm{R}} \\ & - K_u \mathscr{P}_{(5)}^{+} \mathscr{P}_{(5)}^{-} (\alpha_{\mathrm{L}}\rho_{\mathrm{L}} + \alpha_{\mathrm{R}}\rho_{\mathrm{R}})(f_a c_{1/2})(u_{\mathrm{R}} - u_{\mathrm{L}}) \end{aligned} \tag{23}$$

The definition of the polynomial functions $\mathscr{M}_{(4)}^{+}(M_{\mathrm{L}})$, $\mathscr{M}_{(4)}^{-}(M_{\mathrm{R}})$, $\mathscr{P}_{(5)}^{+}$ and $\mathscr{P}_{(5)}^{-}$ may be found in Liou's original work (e.g. [5]). It should be remarked that in this heavy-laden mixture approach, $p_{p,\mathrm{L}}$ and $p_{p,\mathrm{R}}$ are given by

$$p_{p,\mathrm{L}} = p_{\mathrm{L}} + \Sigma_{\mathrm{L}} \tag{24}$$

$$p_{p,\mathrm{R}} = p_{\mathrm{R}} + \Sigma_{\mathrm{R}} \tag{25}$$

where Σ accounts for the particle–particle interaction in those approaches where the solid pressure is defined by an expression similar to Equation (4). This term is defined in the following sections depending on the approach.

In the case of dilute mixtures discussed in the next section, where the effect of particle–particle interaction may be neglected, the same numerical scheme may be applied, regardless of the terms that take it into account. The resulting model is a one-pressure model where $p = p_g = p_p$.

3.2.2. High-dilute mixtures. The system of equations for high-dilute dusty gas flows has a different eigenstructure with respect to System (1). Although the gas sub-system is strictly hyperbolic, the particle system of equations is a degenerate one, it has only one eigenvalue, the particle velocity, u_p with multiplicity 3, so the Jacobian matrix of the flux is not diagonalizable. In the finite volume formulation for this model, the vector of conserved variables and the flux vector are given by

$$U = \begin{bmatrix} \rho_g \\ \rho_g u_{gx} \\ \rho_g u_{gy} \\ \rho_g u_{gz} \\ \rho_g E_g \\ \sigma \\ \sigma u_{px} \\ \sigma u_{py} \\ \sigma u_{pz} \\ \sigma E_p \end{bmatrix}, \quad F = \begin{bmatrix} \rho_g u_{gx} \\ \rho_g (u_{gx}^2 + p) \\ \rho_g u_{gx} u_{gy} \\ \rho_g u_{gx} u_{gz} \\ \rho_g u_{gx} H_g \\ \sigma u_{px} \\ \sigma u_{px}^2 \\ \sigma u_{px} u_{py} \\ \sigma u_{px} u_{pz} \\ \sigma u_{px} E_p \end{bmatrix}, \quad G = \begin{bmatrix} \rho_g u_{gy} \\ \rho_g u_{gy} u_{gx} \\ \rho_g (u_{gy}^2 + p) \\ \rho_g u_{gy} u_{gz} \\ \rho_g u_{gy} H_g \\ \sigma u_{py} \\ \sigma u_{py} u_{px} \\ \sigma u_{py}^2 \\ \sigma u_{py} u_{pz} \\ \sigma u_{py} E_p \end{bmatrix}, \quad H = \begin{bmatrix} \rho_g u_{gz} \\ \rho_g u_{gz} u_{gx} \\ \rho_g u_{gz} u_{gy} \\ \rho_g (u_{gz}^2 + p) \\ \rho_g u_{gz} H_g \\ \sigma u_{pz} \\ \sigma u_{pz} u_{px} \\ \sigma u_{pz} u_{py} \\ \sigma u_{pz}^2 \\ \sigma u_{pz} E_p \end{bmatrix} \tag{26}$$

DOI: 10.1002/fld

In this approximation, S is the source term which groups gravitational effects interfacial friction and interfacial heat transfer.

Different schemes have been applied in the existing literature to solve the system of equations (8). Some authors such as Miura and Glass [16] or Saito [17] proposed random choice methods for its solution assuming a linear distribution for the initial conditions, in order to avoid multivalued solutions for the particle velocity. Other authors use Godunov methods such as Klemens and Kosinski [18] and Klemens *et al.* [19] or Collins *et al.* [20] where a second-order Godunov scheme with adaptive mesh refinement is applied. Saurel *et al.* solve the gas system of equations by means of Van Leer's scheme and the particle system *via* a donor-cell method which uses the solution of a particular Riemann problem [21]. In a similar way, Daniel and Loraud also solve the exact Riemann problem for the flux calculation [22]. Niu applies the AUSMD scheme to the analysis of particulate flow [23]. A $k-\varepsilon$ turbulent model is also included in the system of equations considered. Aiming to solve some imperfections encountered in previous works [24], Abgrall and Saurel introduce a new class of schemes which is able to converge to the correct solution in the presence of shocks and provides a better estimation of the source terms [25]. They apply these schemes to another interpretation of the already presented Baer–Nunziato model.

Gas phase: The AUSM$^+$up scheme is also applied to the gas phase. As the void fraction has been dropped from the system of equations, the flux vector coincides with the Euler flux. Thus the application of this scheme is exactly the same as in the Liou's original work [5]. Another interesting AUSM approach for high-dilute flows can be found in the existing literature [23], in which, Niu reformulates the gas speed of sound in order to overcome some problems found in the cases in which particles are moving with low velocities. In spite of its good results, the AUSM$^+$up has been preferred in this paper as the results obtained have been quite satisfactory.

Solid phase: Due to the degenerate character of the solid system of equations, two options are proposed:

Rusanov scheme: In this case, the numerical flux is computed using the following expression [26]:

$$F_{j+1/2} = \tfrac{1}{2}[(F_{\mathrm{L}} + F_{\mathrm{R}}) - S^{+}(U_{\mathrm{R}} - U_{\mathrm{L}})] \tag{27}$$

where the speed S^+ is chosen such that

$$S^{+} = \max\{|u_{p\mathrm{L}}|, |u_{p\mathrm{R}}|\} \tag{28}$$

AUSM scheme: As there is no pressure term in the particle physical flux, the numerical flux is purely convective. The approximation followed is equivalent to that formulated by Niu [23]. As the solid phase is considered incompressible and the solid speed of sound is constant, AUSM fluxes are redefined in terms of a numerical particle velocity at the interface

$$F_{j+1/2} = \dot{u}_{p1/2} \begin{cases} \psi_{\mathrm{L}} & \text{if } \dot{m}_{p1/2} \geqslant 0, \\ \psi_{\mathrm{R}} & \text{otherwise,} \end{cases} \qquad \psi = \begin{bmatrix} \sigma \\ \sigma u_{pn} \\ \sigma u_{pt_1} \\ \sigma u_{pt_2} \\ \sigma E_p \end{bmatrix} \tag{29}$$

where the numerical particle velocity is defined as

$$u_{p1/2} = \tfrac{1}{2}(u^{+}_{p\mathrm{L}} + u^{-}_{p\mathrm{R}}) \tag{30}$$

DOI: 10.1002/fld

and $u_p^{\pm} = \frac{1}{2}(u_p \pm |u_p|)$. A version of the AUSM+ scheme under the previously mentioned consideration of particle incompressibility was also developed. The results provided are, however, somewhat oscillatory with respect to the version described and they have not been included for reason of clarity.

3.3. Second-order approximation

A second-order scheme can be obtained by using the MUSCL-variable extrapolation strategy. In the code developed, the following algorithm has been followed.

Prediction step: The primitive variables are calculated at a time step $\Delta t/2$ by means of

$$\tilde{V}_j^{n+1/2} = V_j^n + A_j \frac{\partial V}{\partial x} + B_j \frac{\partial V}{\partial y} + C_j \frac{\partial V}{\partial z} \tag{31}$$

This has been obtained by writing the homogeneous system of System (8) as

$$\frac{\partial U}{\partial t} + \frac{\partial F}{\partial x} + \frac{\partial F}{\partial y} + \frac{\partial F}{\partial z} = 0 \tag{32}$$

transforming it into

$$\frac{\partial V}{\partial t} + A\frac{\partial V}{\partial x} + D\frac{\partial V}{\partial y} + C\frac{\partial V}{\partial z} = 0 \tag{33}$$

after doing some algebra. Matrices A, B and C stand for $(\partial U/\partial V)^{-1}\partial F/\partial V$, $(\partial U/\partial V)^{-1}\partial G/\partial V$ and $(\partial U/\partial V)^{-1}\partial H/\partial V$, respectively.

Correction step: The previously calculated primitive variables are reconstructed in space by means of

$$\bar{V}_j = \tilde{V}_j + (\nabla \tilde{V})_j \cdot (\mathbf{r} - \mathbf{r}_j) \tag{34}$$

where $\mathbf{r}$ is the vector characterizing the position of the points considered in the reconstruction process.

Conserved variable update: Finally, conserved variables are updated by means of

$$U_j^{n+1} = U_j^n - \frac{\Delta t}{|V|} \sum_{s=1}^{N} T_s^{-1} F(T_s \bar{U}) A_s \tag{35}$$

where the numerical fluxes are obtained by any of the numerical schemes proposed prior to this by using the previously calculated linearized primitive variables. Gradients have been approximated by means of the method introduced by Beccantini and Paillère [27] and limited by using a version of the Barth–Jespersen limiter, also used in this reference.

4. NUMERICAL RESULTS

Some numerical tests are studied with the aforementioned schemes. Despite the multidimensional character of the development presented above, most of the problems studied are essentially 1D, as they will allow us to check the behaviour of the schemes in the presence of discontinuities or rather

DOI: 10.1002/fld

strong gradients. The system of equations used to model dust and gas mixtures is quite similar to that used for two-fluid and two-phase mixtures, this development takes advantage of previous experiences in the application of advected upstream schemes to problems with gas and liquid mixtures (i.e. [4, 28]). Problems with both heavy-laden and high-diluted mixtures are studied. The high-dilute approach is used for problems with very high gas volume fractions, where particle–particle interaction is neglected and only drag and heat transfer between the phases are taken into account. All simulations are performed using the CAST3M code [29]. This is a multi-purpose finite element code, developed at the CEA (French Atomic Commission). Its domains of application are Structural Mechanics, Fluid Mechanics, Thermal Engineering and Electromagnetism. It is quite flexible and allows the user to post-process the results. This is an open code, may be modified and new code may also be added.

4.1. Heavy-laden mixtures

Two tests are studied. The system of equations solved and the interaction terms included in them follow the original references. The first one is a four-equation model studied by Combe and Hérard [9, 30] and the second is a six-equation model analysed by Rogue *et al.* [12].

4.1.1. Four-equation model. Combe and Hérard studied a four-equation model for laden mixtures of gas and particles, following the model studied by Gidaspow [1]. In this approach, neither the particle volume fraction transport equation nor the energy equations of System (1) are considered. Particle interaction is taken into account by writing the particle pressure as the sum of the gas pressure and the so-called intergranular pressure Σ. This results in the following system of equations:

$$\begin{gathered}
\frac{\partial}{\partial t}(\alpha\rho_g) + \nabla\cdot(\alpha\rho_g\mathbf{u}_g) = 0 \\
\frac{\partial}{\partial t}(\alpha\rho_g\mathbf{u}_g) + \nabla\cdot(\alpha\rho_g\mathbf{u}_g\otimes\mathbf{u}_g + \alpha p) = p\nabla\alpha + \alpha\rho_g g + \phi_g^{nv} + \phi_g^{v} \\
\frac{\partial}{\partial t}((1-\alpha)\rho_p) + \nabla\cdot((1-\alpha)\rho_p\mathbf{u}_p) = 0 \\
\frac{\partial}{\partial t}((1-\alpha)\rho_p\mathbf{u}_p) + \nabla\cdot((1-\alpha)\rho_p\mathbf{u}_p\otimes\mathbf{u}_p + (1-\alpha)(p+\Sigma)) \\
= -p\nabla\alpha + \alpha\rho_p g + \phi_p^{nv} + \phi_p^{v}
\end{gathered} \tag{36}$$

where $p = p(\rho_g)$ is the mean pressure within the gas phase given by the equation of state at constant entropy

$$p = \kappa\rho_g^{v} \tag{37}$$

where κ and v are two characteristic constants of the gas.

Σ is the intergranular pressure given by

$$\Sigma = \tfrac{2}{3}\rho_p(q_p^2)_0(\alpha_p)^{5/3}g(\alpha_p) \tag{38}$$

DOI: 10.1002/fld

Figure 1. Shock tube test specifications with zero velocities.

Figure 2. Shock tube test specifications with opposite velocities.

ρ_p is constant as the solid phase is considered incompressible:

$$g(\alpha_p) = \left[1 + \frac{2(1+e_c)\alpha_p}{[1-\alpha_p/\alpha_{\max}]^{\frac{5}{3}\alpha_{\max}}}\right] \exp\left[\frac{4\alpha_{\max}(1+e_c)}{(\frac{15}{2})\alpha_{\max} - 3}\left(1 - \frac{\alpha_p}{\alpha_{\max}}\right)^{1-\frac{5}{2}\alpha_{\max}}\right]$$

$\alpha_{\max} = 0.64$ maximum particle compactness rate, assuming they are spherical, $e_c = 1$, $(q_c^2)_0 = 15/2$ (it is a constant of dimension $(\mathrm{m\,s^{-1}})^2$ [30]) and α_p is the particle volume fraction is $\alpha_p = 1 - \alpha$.

The speeds of sound of the phases are given by

$$c_g^2 = \frac{\mathrm{d}p_g}{\mathrm{d}\rho_g}, \quad c_p^2 = \frac{\mathrm{d}\Sigma}{\mathrm{d}\alpha_p} \tag{39}$$

Two shock tube problems are studied (Figures 1 and 2). In both cases, the particle density is taken as constant and the particle diameter $d_p = 10^{-4}$ m. The perfect gas equation of state is given by $\kappa = 10^5$ Pa and $\nu = 7/5$. The first problem is a shock tube with drag whose left and right states are characterized by the following values for the conserved variables (Figure 5):

$$U_{\mathrm{L}} = \begin{bmatrix} \alpha\rho_g = 0.5 \\ \alpha\rho_g u_g = 0 \\ (1-\alpha)\rho_p = 1250 \\ (1-\alpha)\rho_p u_p = 0 \end{bmatrix}, \quad U_{\mathrm{R}} = \begin{bmatrix} \alpha\rho_g = 0.12 \\ \alpha\rho_g u_g = 0 \\ (1-\alpha)\rho_p = 1500 \\ (1-\alpha)\rho_p u_p = 0 \end{bmatrix} \tag{40}$$

and the value of the particle density is $\rho_p = 2500\,\mathrm{kg/m^3}$.

The second problem is given by the following values of the conserved variables. In this case, the value of the particle density is $\rho_p = 2500\,\mathrm{kg/m^3}$.

$$U_{\mathrm{L}} = \begin{bmatrix} \alpha\rho_g = 0.5 \\ \alpha\rho_g u_g = 350 \\ (1-\alpha)\rho_p = 1250 \\ (1-\alpha)\rho_p u_p = 6250 \end{bmatrix}, \quad U_{\mathrm{R}} = \begin{bmatrix} \alpha\rho_g = 0.5 \\ \alpha\rho_g u_g = -350 \\ (1-\alpha)\rho_p = 1250 \\ (1-\alpha)\rho_p u_p = -6250 \end{bmatrix} \tag{41}$$

DOI: 10.1002/fld

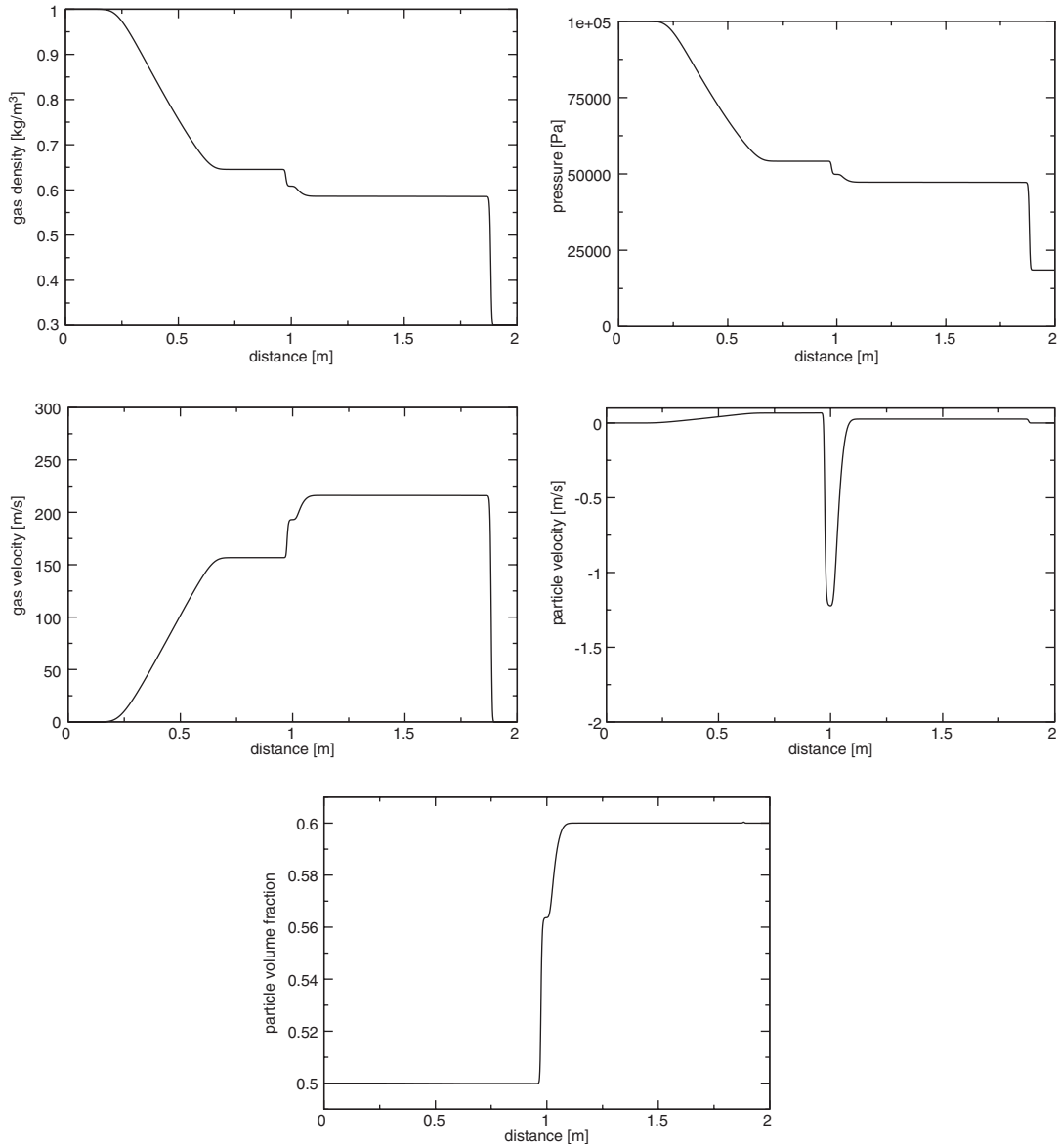

Figure 3. Shock tube with drag. From top to bottom, left to right: gas density, pressure, gas velocity, particle velocity and particle volume fraction.

This differs from the former since the phases have opposite velocities which will lead to an increase of the particle concentration in the middle of the tube.

For these tests, a simplified version of the particle intergranular pressure defined in Equation (38) is used:

$$\alpha_p \Sigma = \beta (q_p^2)_0 \frac{\alpha_p}{1 - \alpha_p / \alpha_{\max}} \tag{42}$$

DOI: 10.1002/fld

In this case, the speeds of sound are given by

$$c_g^2 = \frac{\mathrm{d}p_g}{\mathrm{d}\rho_g} = \kappa v \rho_g^{v-1}, \quad c_p^2 = \frac{\mathrm{d}\Sigma}{\mathrm{d}\alpha_p} = \frac{\alpha_{\max}^2 \beta (q_p^2)_0}{(\alpha_{\max} - \alpha_p)^2} \tag{43}$$

$\beta = \frac{2}{3}$, $\alpha_{\max} = 0.64$ and $(q_p^2)_0 = 5$.

The drag force is the only phase interaction term considered in the calculations and the model used is given by

$$\mathbf{F}_d = -\alpha(1-\alpha) K_T (\mathbf{u}_g - \mathbf{u}_p) \tag{44}$$

where

$$K_T = \begin{cases} \dfrac{3}{4}\dfrac{C_d}{d_p}\rho_g \alpha^{-2.7} |\mathbf{u}_g - \mathbf{u}_p| & \text{if } \alpha_p < 0.2 \\ \dfrac{\rho_g}{\alpha d_p}\left((1-\alpha)\dfrac{150}{Re} + 1.75\right)|\mathbf{u}_g - \mathbf{u}_p| & \text{otherwise} \end{cases} \tag{45}$$

with $Re = \alpha d_p |\mathbf{u}_g - \mathbf{u}_p| / v_g$ and

$$C_d = \begin{cases} \dfrac{24}{Re}(1 + 0.15 Re^{0.7}) & \text{if } Re < 1000 \\ 0.44 & \text{otherwise} \end{cases}$$

The gas kinematic viscosity is $v_g = 10^{-5}\,\mathrm{m}^2/\mathrm{s}$.

These tests are studied by applying the already described AUSM$^+$up formulation for dense mixtures. The calculations have been performed using a 1D mesh of 1500 cells and a CFL-like parameter of 0.9. In Figure 3, the results corresponding to the shock tube with drag have been gathered. Similarly, the numerical results corresponding to the shock tube with opposite velocities have been displayed in Figure 4. These results are quite similar to those reported by Combe and Hérard [9, 30], there are some differences as the exact time at which the data were represented was not reported in these references. Figures 3 and 4 correspond to $t = 2$ and 1.5 ms, respectively. In the first test, the velocity and void fraction of the particles are not affected by the rarefaction and the shock wave in the gas phase. Instead, gas density and velocity are very influenced by the particle existence compared with what occurs when we have got only gas. In the second test, kinetic energy is converted into pressure within each phase in the central region. As it is expected, it results in an increase of the void fraction.

4.1.2. Six-equation model. Rogue *et al.* studied the fluidization of different particle beds both by experimental and analytical methods [12]. The model considered in their work is characterized by

DOI: 10.1002/fld

the following system of equations:

$$\begin{aligned}
\frac{\partial \alpha_g \rho_g}{\partial t} + \nabla(\alpha_g \rho_g u_g) &= 0 \\
\frac{\partial \alpha_g \rho_g u_g}{\partial t} + \nabla(\alpha_g \rho_g u_g^2 + \alpha_g p_g) &= p\nabla(\alpha_g) + F_d \\
\frac{\partial \alpha_g \rho_g E_g}{\partial t} + \nabla(\alpha_g \rho_g u_g H_g) &= Q + F_d u_p \\
\frac{\partial \alpha_p \rho_p}{\partial t} + \nabla(\alpha_p \rho_p u_p) &= 0 \\
\frac{\partial \alpha_p \rho_p u_p}{\partial t} + \nabla(\alpha_p \rho_p u_p^2 + \alpha_p p_p) &= -p\nabla\alpha_p - F_d \\
\frac{\partial \alpha_p \rho_p E_p}{\partial t} + \nabla(\alpha_p \rho_p u_p (E_p + p_p/\rho_p)) + &= -Q - F_d u_p
\end{aligned} \tag{46}$$

it is a one-pressure model which is in fact the result of considering only a weak compaction in System 1. This is $p_p = p_g + \tilde{T}$ (with $\tilde{T}$ the particle interaction tensor). The gas phase is modelled as a perfect gas and the solid phase is considered to be incompressible as before. The subscript g stands for the gas phase and p for the solid one as usual $\alpha_g + \alpha_p = 1$, Q is the convective heat transfer between the phases and F_d is the interfacial friction force. This test was also studied by Abgrall and Saurel [25]. The numerical results shown by these authors match quite well the experimental results.

In this section, the fluidization effect of a shock induced on a particle bed is numerically studied and compared to the experimental results obtained by Rogue *et al.* In essence, the problem consists of a particle bed situated inside a vertical tube in which the flow is driven upwards by a shock. In the experimental study, the authors analysed different particle beds which ranged from one particle to compact beds, characterized by different particle volume fractions. Furthermore, they tested several types of particles (nylon and glass) under the action of distinct shocks (Mach numbers from 1.3 to 1.5). The geometry specifications are shown in Figure 5.

In the present case, aimed at validating this development, a test with glass is carried out, the shock considered is given by a Mach number of 1.3 and the initial conditions are:

- *Driven part*: a density and a pressure of $\rho_g = 1.2\,\mathrm{kg/m^3}$ and $p = 10^5\,\mathrm{Pa}$ are, respectively, considered. The particle bed is characterized by a gas volume fraction of 0.35.
- *Driver part*: By taking into account the above values and by solving Rankin–Hugoniot jump conditions for a shock velocity characterized by a Mach number of 1.3, the following values are obtained in the driven part of the tube: $\rho_g = 1.82\,\mathrm{kg/m^3}$, $p = 180\,500\,\mathrm{Pa}$ and $u_g = 151.1\,\mathrm{m/s}$. Besides, for the glass a density of $\rho_p = 2500\,\mathrm{kg/m^3}$ and a particle diameter of $d_p = 1.5\,\mathrm{mm}$ is set.

  The interfacial friction is characterized by the following drag force expression:

$$\mathbf{F}_{dg} = -\frac{3}{4} C_d \frac{\rho_g}{d_p}(1 - \alpha_g)|\mathbf{u}_g - \mathbf{u}_p|(\mathbf{u}_g - \mathbf{u}_p) \tag{47}$$

DOI: 10.1002/fld

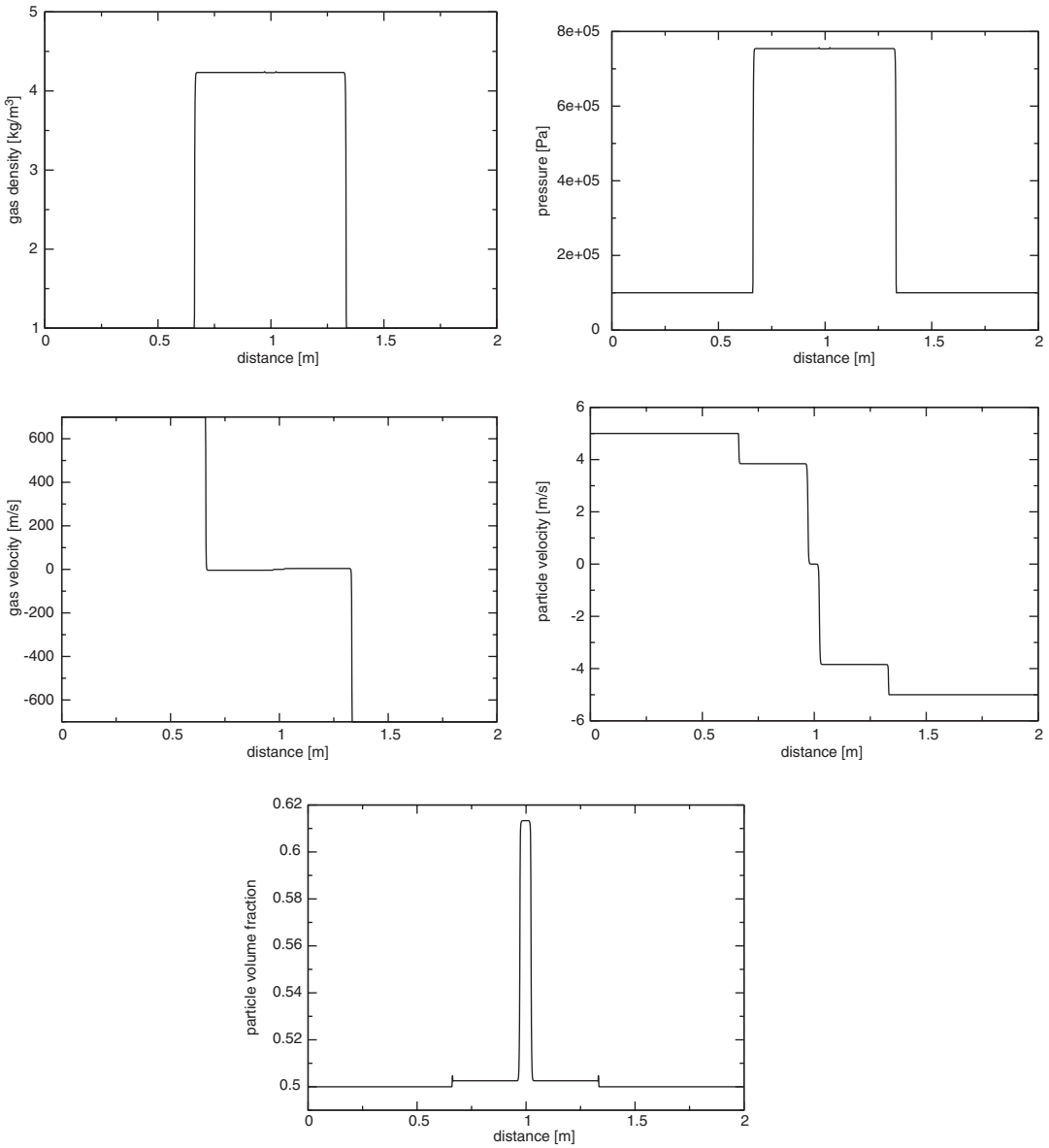

Figure 4. Shock tube without drag and opposite velocities. From top to bottom, left to right: gas density, pressure, gas velocity, particle velocity and particle volume fraction.

$C_d = 0.6$ is a constant drag coefficient and $c_m = 951.36\,\mathrm{J/(kg\,K)}$ is the specific heat of glass at constant volume which is set following the problem definition in [12]. Considering these values, the particle concentration in the bed is $\sigma = (1 - \alpha_g)\rho_p = 682.5\,\mathrm{kg/m^3}$.

DOI: 10.1002/fld

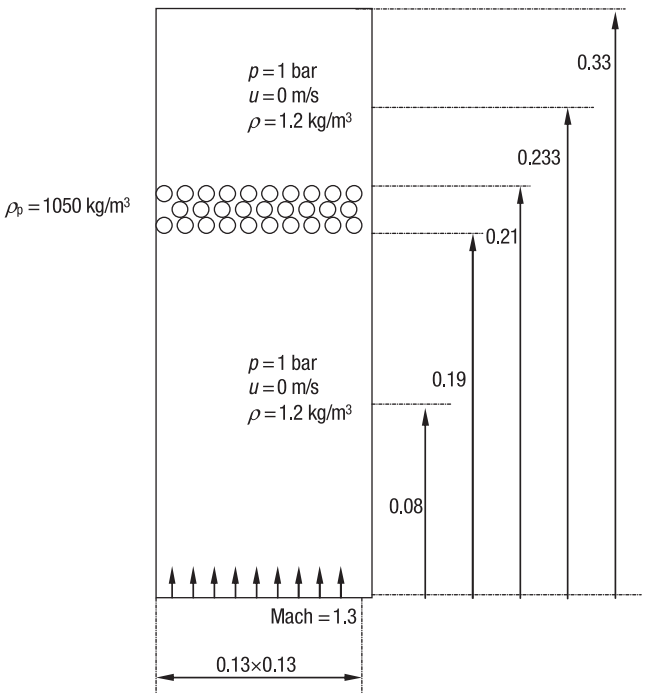

Figure 5. Fluidization particle bed test. Geometrical specifications.

The interfacial heat transfer is expressed by

$$Q = \pi d_p (1 - \alpha) \lambda_g Re^{0.7} Pr^{0.33} (T_p - T_g) \tag{48}$$

where Pr is the Prandtl number of the gas phase and the Reynolds number is given by $Re = (\rho_g |\mathbf{u}_g - \mathbf{u}_p| d_p)/\mu_g$. The interaction term is given by

$$\tilde{T} = \rho_p c_{s0}^2 \left(1 - \frac{\alpha_{s0}}{\alpha_p}\right) \tag{49}$$

which is supposed to be dependent only on the compaction rate. The speed of sound expression is obtained following [11]

$$c_p^2 = \frac{1}{\rho_p} \frac{\mathrm{d}}{\mathrm{d}\alpha_p} [\alpha_p (p_g + \tilde{T})] = c_{s0}^2 + \frac{p}{\rho_p} \tag{50}$$

where c_{s0}=200 m/s has been estimated considering similar experiments and α_{s0}=0.35 in this case.

The results obtained at the two gauge positions and for a particle bed of 2 cm in thickness are gathered in Figure 6. They are quite similar to those shown by Rogue *et al.* [12] although they differ somewhat from the experimental results, referred to as 'pexp' in the figures. When the shock meets the particle bed, the particles get fluidized and, later a shock with a higher pressure than the initial one is reflected towards the bottom and a low pressure one is transmitted through the particle bed. The reflected shock is lower than in the experiment. On the other hand, the transmitted

DOI: 10.1002/fld

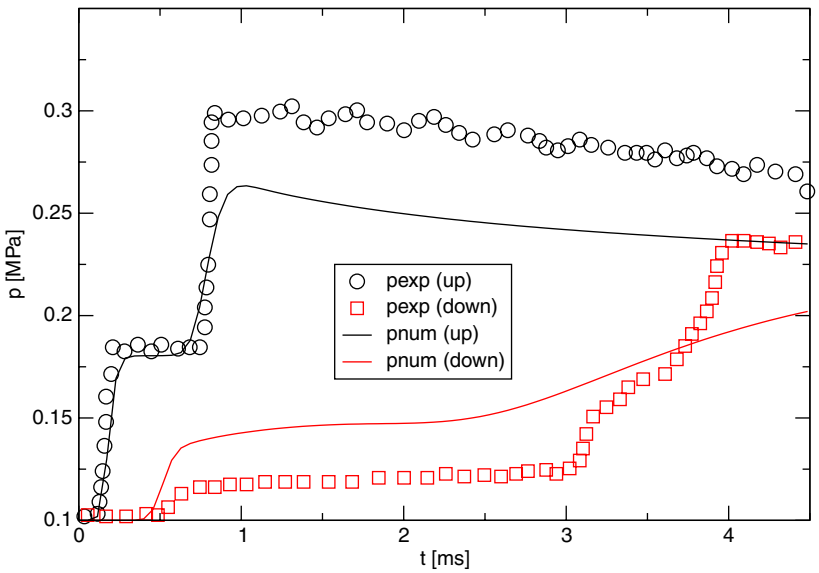

Figure 6. Gauge pressure at two different positions from the particle bed (bed thickness 2 mm).

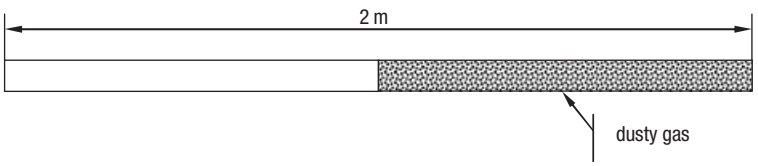

Figure 7. Shock tube problem geometry.

shock is stronger which makes the gas flow faster through the bed. Perhaps, this is due to certain numerical diffusion and the fact that the grid is not being modelled. A sensitivity study has been carried out varying the time step and the grid points but no special improvement has been obtained. The differences encountered between the experimental and the calculated results might be due to the simplified model used to characterize the particle–particle interaction.

4.2. High-dilute mixtures

In this section, two test cases are studied. One corresponds to a shock tube introduced by Miura and Glass [16] whilst the other is a version of the problem studied by Klemens *et al.* [31], where a rarefaction wave mobilizes a dust layer situated on the bottom of a vertical tube.

4.2.1. Shock tube test. It consists of a 2 m long horizontal tube divided into two parts by a membrane (Figure 7). This separates a left zone (driver part) containing only air at high pressure, and a right zone (driven part), which has a mixture of particles and air with lower pressure (8).

DOI: 10.1002/fld

Initial conditions are given by the following left and right states:

$$V_{\mathrm{L}} = \begin{bmatrix} p = 10^6\,\mathrm{Pa} \\ u_g = u_p = 0\,\mathrm{m/s} \\ T_g = T_p = 300\,\mathrm{K} \\ \sigma = 0\,\mathrm{kg/m^3} \end{bmatrix}, \quad V_{\mathrm{L}} = \begin{bmatrix} p = 10^5\,\mathrm{Pa} \\ u_g = u_p = 0\,\mathrm{m/s} \\ T_g = T_p = 300\,\mathrm{K} \\ \sigma = \rho_g(10^5\,\mathrm{Pa}, 300\,\mathrm{K})\,\mathrm{kg/m^3} \end{bmatrix} \tag{51}$$

In this test, the gas is considered to be perfect, viscous friction and conduction heat transfer effects are neglected, and particles are assumed to be spherical with uniform size as is commented above. The interaction between the phases is characterized by a drag force given by

$$F_d = -\frac{\sigma}{m} D \tag{52}$$

and an interfacial heat transfer term

$$Q_g = -\frac{\sigma}{m} Q \tag{53}$$

which takes into account the convection heat transfer between the gas and the particles, in such a way that

$$D = \tfrac{1}{8}\pi d_p^2 \rho_g (u_g - u_p)|u_g - u_p| C_d \tag{54}$$

$$Q = \pi d_p v c_{pg} Pr^{-1} (T_g - T_p) Nu \tag{55}$$

with the particle diameter denoted by d_p and the drag coefficient, C_d given by

$$C_d = 0.48 + 28 Re^{-0.85} \tag{56}$$

the Nusselt number, Nu, by

$$Nu = 2 + 0.6 Pr^{1/3} Re^{1/2} \tag{57}$$

and the Reynolds number, Re, is based on the particle diameter d_p and the relative velocity between the phases:

$$Re = \frac{\rho_g |u_g - u_p|}{\mu_g} \tag{58}$$

Prandtl number is given by $Pr = (\mu_g c_p)/k_g$ and the gas dynamic viscosity by means of $\mu_g = 1.71 \times 10^{-5}(T_g/273)^{0.77}\,\mathrm{Ns/m^2}$. k_g is the thermal conductivity of the gas phase and m is the particle mass assuming it spherical. These closure expressions follow Otterman and Levinet's work [32].

In order to test the ability of the schemes to capture a shock wave, several studies are carried out. Firstly, grid independence is shown varying the number of cells considered from 100 to 10 000. The distribution of some representative variables along the tube are depicted in Figures 8 and 9. These are pressure, gas density, particle concentration, gas and particle temperature, and gas and particle velocities. All these results correspond to numerical calculations carried out by means of the AUSM$^+$up scheme for the gas and the Rusanov scheme for the particles.

In Figure 10, a mesh of 1000 cells in the main axis is used. Here, the results corresponding to the test described above are compared to those obtained considering the same problem but

DOI: 10.1002/fld

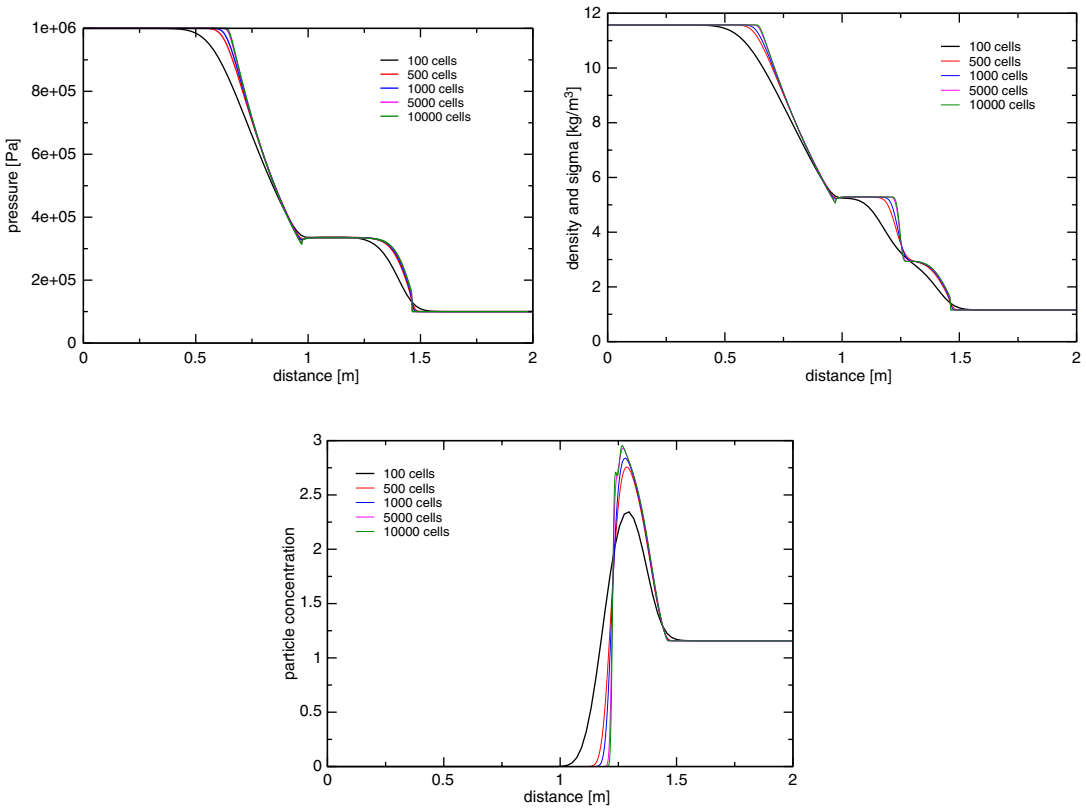

Figure 8. Shock tube problem: from left to right, top to bottom: pressure, gas density, and particle concentration.

with only gas. This single-phase results have been obtained by employing the AUSM^{+}up scheme for the Euler equations in this shock problem with the specifications given above. They show the differences encountered between the mixture and the single-phase behaviours. These results are essentially the same as those shown by the referenced authors [16, 17]. Particle concentration increases very slowly behind the shock reaching a maximum and dropping behind the contact discontinuity. Gas velocity is lower than that in the single-phase case due to the gas–particle interaction. Gas loses energy which results in a shock deceleration. It produces compression waves behind the shock wave and a consequent increase in pressure. We notice that the rarefaction is reduced and temperature does not decrease as much as in the single-phase case. The oscillations avoided by the numerical scheme proposed by Saito do not appears either in the case of the numerical scheme proposed in this paper.

A comparison of the results obtained by means of the first-order and second-order version of the scheme has also been depicted in Figure 11.

4.2.2. Dust mobilization due to rarefaction waves. This test case was experimentally studied by Medvedev *et al.* [33] and studied numerically by Klemens *et al.* [31] and Klemens and

DOI: 10.1002/fld

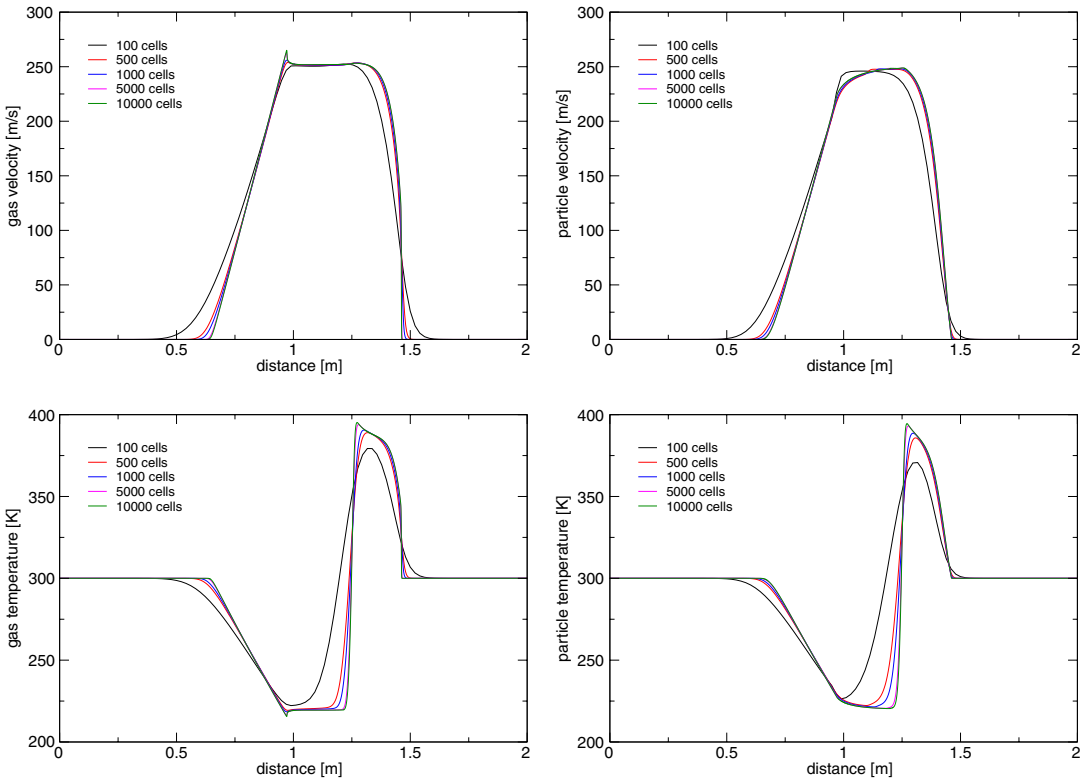

Figure 9. Shock tube problem: from left to right, top to bottom: gas and particle velocity, and gas an particle temperature.

Kosinski [18]. It simulates the dispersion of a dust layer due to the action of rarefaction waves. It consists of a long tube which has a 50 mm dust deposit which is subjected to high pressure on its left side (Figure 12).

On the upper part of the tube, there is a low-pressure region, with an arbitrary length which is separated from the first part by a membrane. Initial conditions are ambient temperature in both parts ($t = 25°\mathrm{C}$), a 2 bar pressure inside the bottom section and 1 bar in the other. The phases are supposed initially at rest. The other parameters that complete the problem definition are the particle concentration $\sigma = 760\,\mathrm{kg/m^3}$, its density $\rho_p = 1300\,\mathrm{kg/m^3}$ and its diameter $d_p = 10^{-5}$ m. Air is considered as a perfect gas and the solid phase is incompressible as mentioned above.

The relationships chosen to close the system of equations are those used by the authors in the references mentioned above which correspond to the correlations proposed by Crowe *et al.* [6]. The drag interaction between the phases is modelled by means of

$$\mathbf{F}_{dg} = -n\frac{\pi d_p^2}{C_d} 4\rho_g |\mathbf{u}_g - \mathbf{u}_p|(\mathbf{u}_g - \mathbf{u}_p) \tag{59}$$

where n is the number of particles per unit volume given by $n = d_p(1-\alpha_g)/m_p$ and C_d is the drag coefficient. Although it was not defined in the previous references, the Schiller and Naumann

DOI: 10.1002/fld

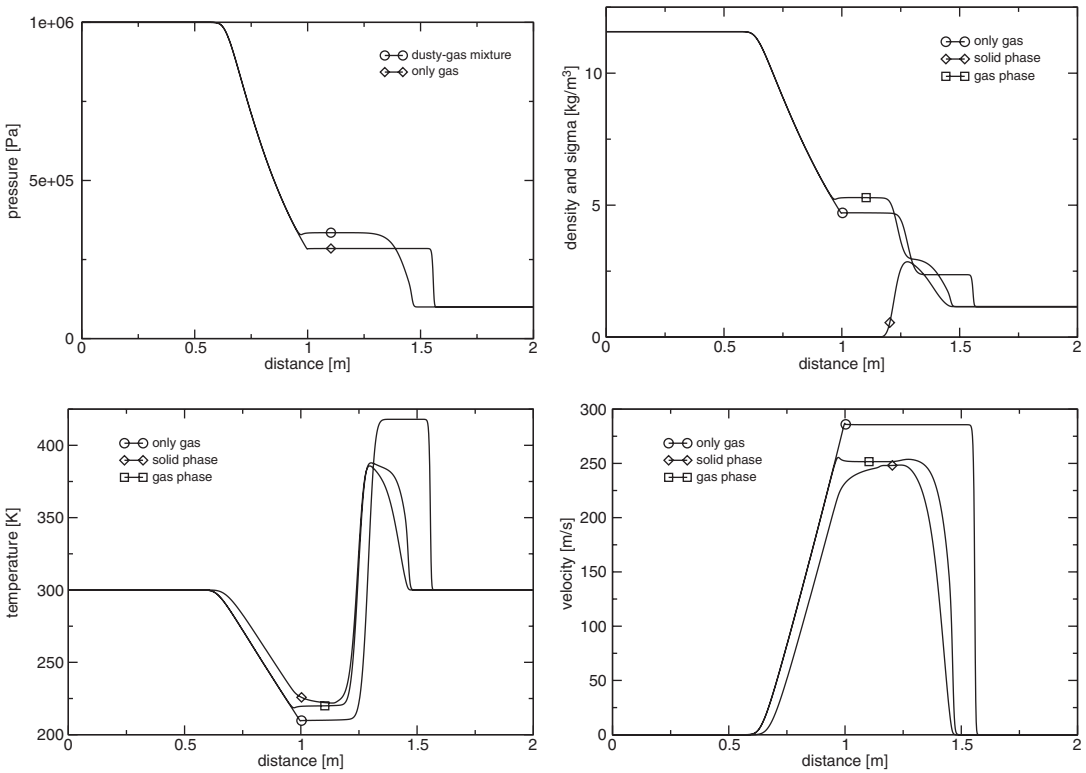

Figure 10. Shock tube problem: from left to right, top to bottom: pressure, density, temperature and velocity.

correlation proposed in [6] has been considered:

$$C_d = (1 + 0.15Re^{0.687}) \tag{60}$$

The heat exchanged through the interface is evaluated with the following expression:

$$Q = n\pi d_p^2 \frac{\lambda_g Nu}{d_p}(T_g - T_s) \tag{61}$$

where the Nusselt number is defined as

$$Nu = 2 + 0.6Pr^{1/3}Re^{1/2} \tag{62}$$

The results shown in Figure 13 have been obtained by means of the AUSM$^+$up scheme for the gas phase and the modified AUSM scheme for the particles. They correspond to the distribution of the particle concentration along the tube for different instants, $t = 0, 2, 4, 6, 8$, and 10 ms. The numerical results shown match quite well with those reported by Klemens *et al.* [31]. In addition, the evolution of the particle concentration is displayed in Figure 14 at different positions: 6.25, 12.5, 18.75 and 25 mm over the dust layer.

DOI: 10.1002/fld

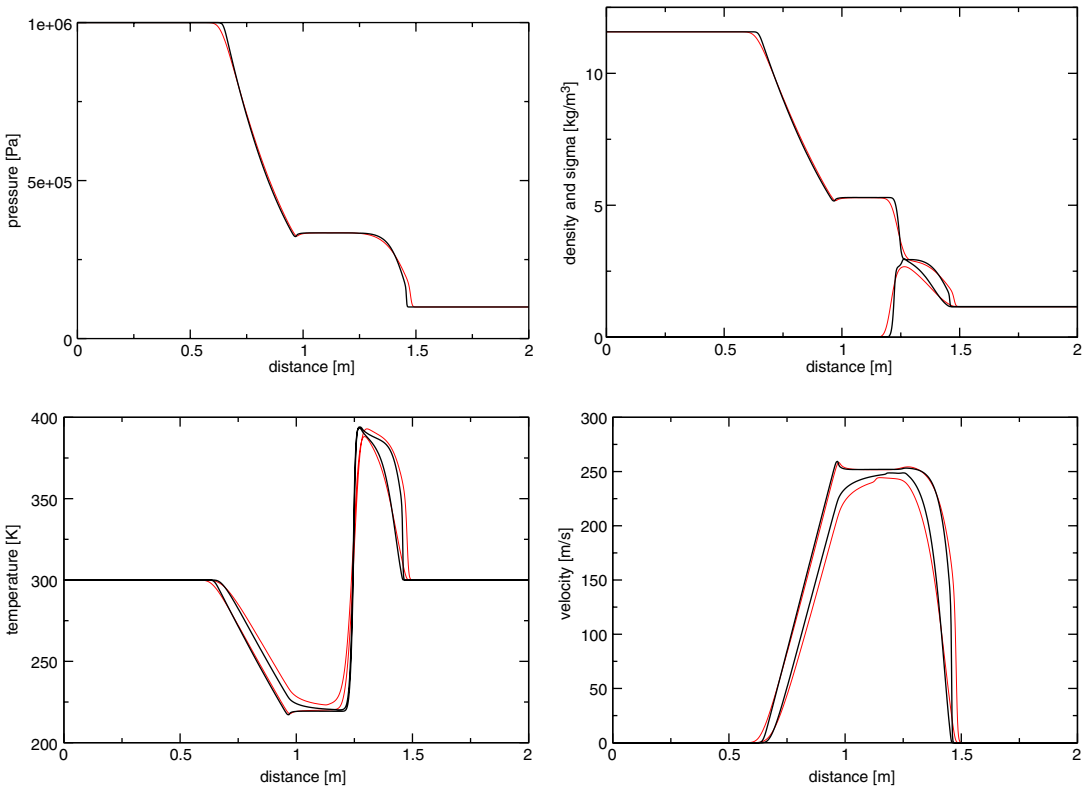

Figure 11. Shock tube problem. Comparison between first order (red) and second order (black). From left to right, top to bottom: pressure, density, temperature and velocity.

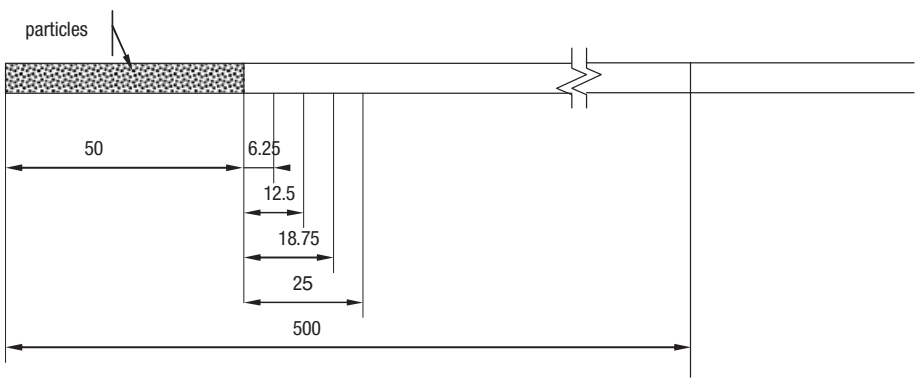

Figure 12. Dust mobilization problem. Geometry specifications, all in mm.

DOI: 10.1002/fld

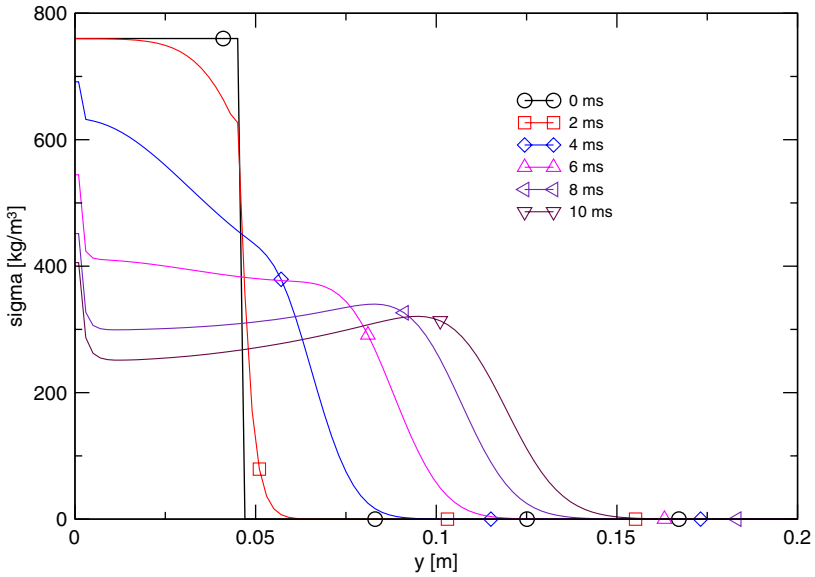

Figure 13. Dust concentration distribution at different times. High dilute mixture model.

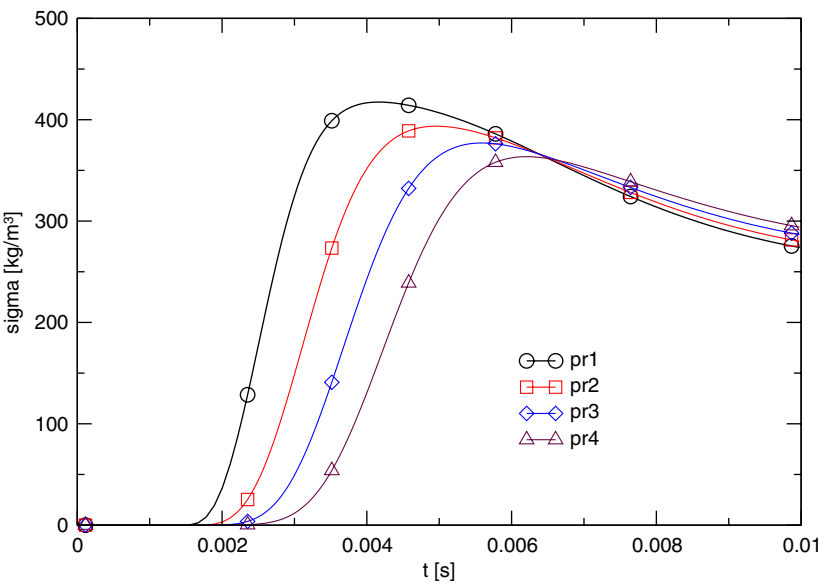

Figure 14. Dust concentration distribution at different times. High dilute mixture model.

DOI: 10.1002/fld

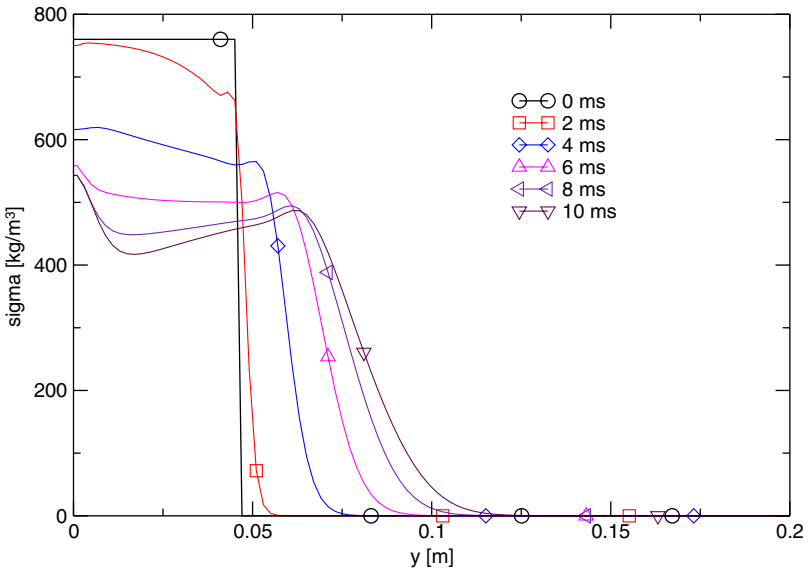

Figure 15. Dust concentration distribution at different times. Dense mixture model.

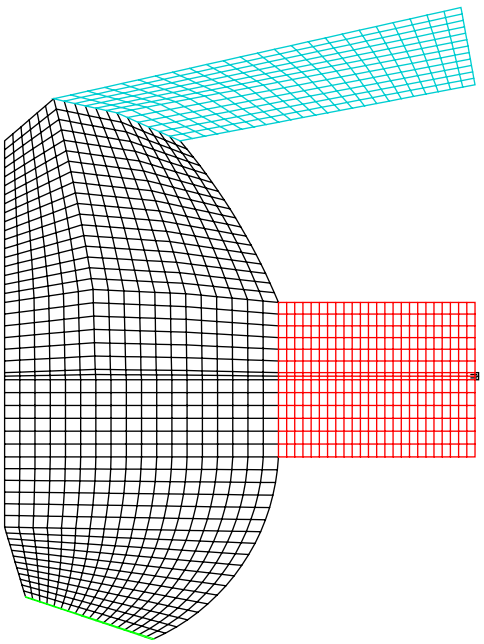

Figure 16. Geometry considered in the analysis.

DOI: 10.1002/fld

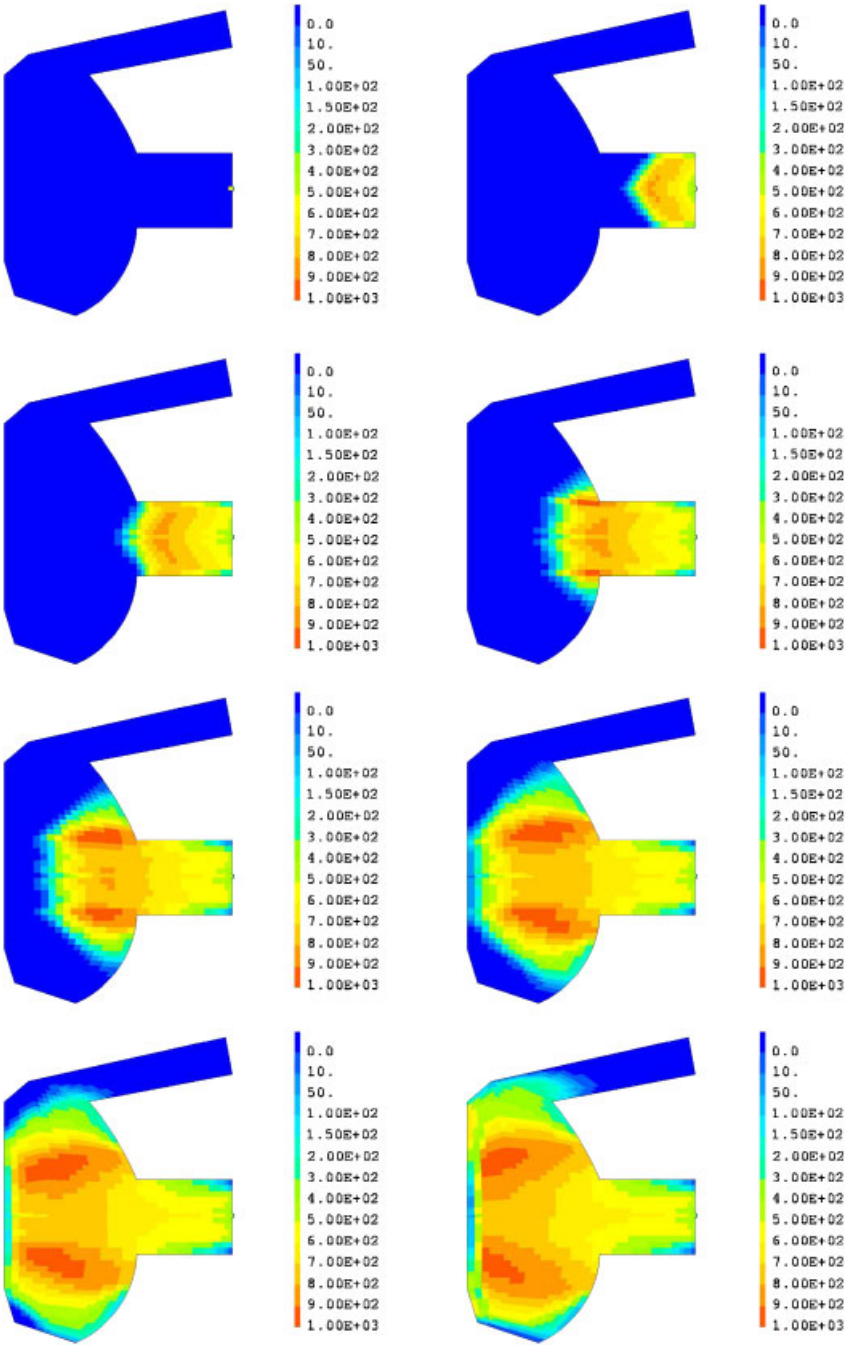

Figure 17. Gas velocity distribution inside the reservoir at different times, $t = (0, 1, 2, 3, 4, 5, 6, 7) \times 10^{-2}$ s.

DOI: 10.1002/fld

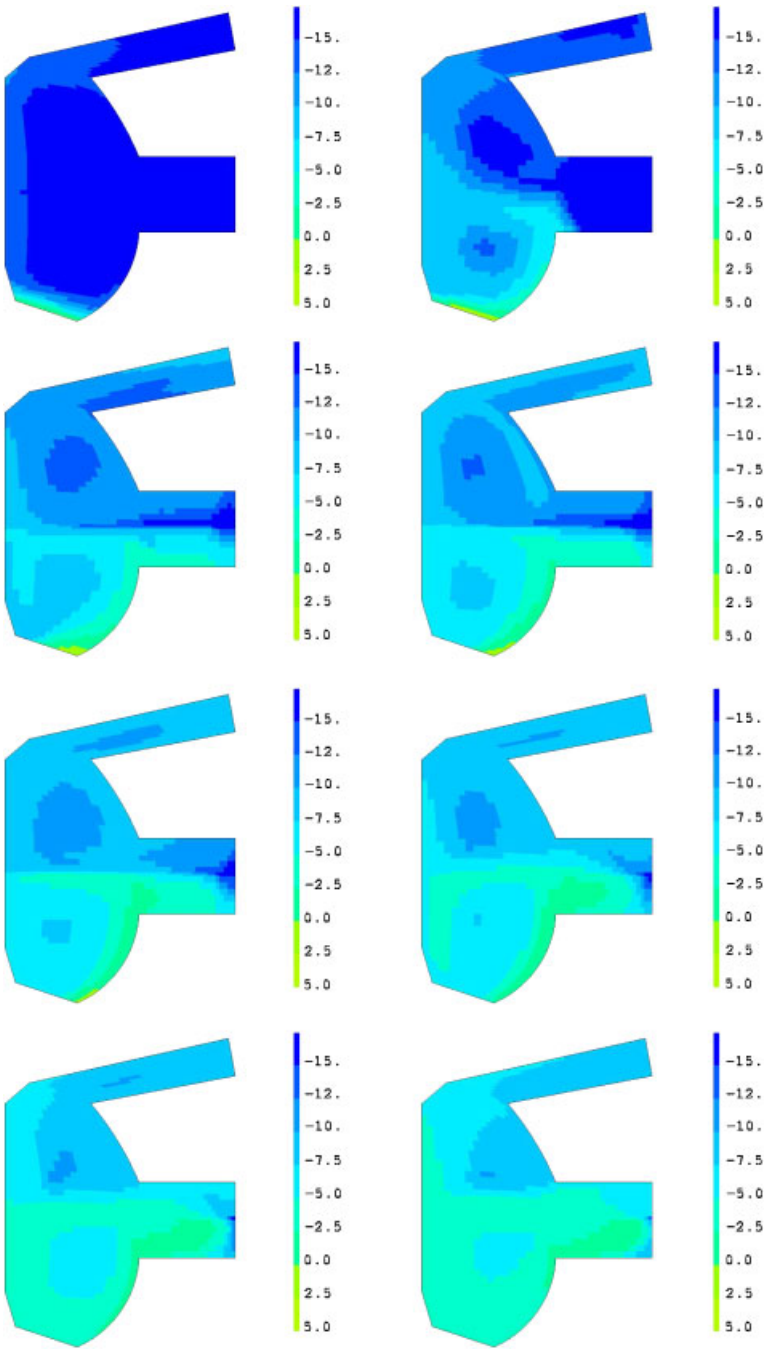

Figure 18. Logarithmic representation of the particle concentration distribution inside 2D ITER cross-section at different times, $t = (0, 1, 2, 3, 4, 5, 6, 7) \times 10^{-2}$ s.

DOI: 10.1002/fld

For the sake of comparison, this test is also studied with the dense flow model. The results obtained are shown in Figure 15. The interfacial friction and the particle–particle interaction is modelled by using the same correlations as those used in the fluidization test proposed by Rogue *et al.* The role played by the interaction terms is appreciated quite well when compared with the previous results, the dust mobilization is somewhat slower in this case than in the first one because of the strong interaction between the particles which slows down the front propagation in the particle concentration. The calculations have been performed by means of the AUSM$^+$up scheme. A mesh of 2000 points in the y-axis direction has been used for all the cases studied.

The influence of the rarefaction wave is clearly seen as it mobilizes the particle as soon as it reaches the dust layer. Regarding the numerical method performance in the high-dilute case, the modified AUSM and the Rusanov schemes applied to the particles give similar results, although only the AUSM results have been included for this test.

4.2.3. Mobilization of a dust layer in simplified 2D ITER cross-section. A study of dust mobilization inside a simplified 2D ITER cross-section has been carried out as preliminary calculations (it does not include the divertor part and the lower port). The geometry considered is shown in Figure 16. A layer of dust have supposed to be deposited on the lower part of the inner surface. After opening a breach in the middle point of the equatorial port, the dust mobilization takes place due to the action of the induced shock wave.

Constant stagnation conditions have been considered along the calculations, $p_0 = 10^5$ Pa and $T_0 = 298$ K. Initially, a thin layer of particles of 1-cm thick is assumed to be at the bottom of the cross-section which is characterized by an arbitrary concentration of $\sigma = 80\,\mathrm{kg/m^3}$. The particles are characterized by the following parameters:

$\rho_p = 2267\,\mathrm{kg/m^3}$.
$c_m = 8.53\,\mathrm{J/(mol\,K)}$ (specific heat at constant volume, (S)).
$d_p = 0.042 \times 10^{-6}\,\mathrm{m}$ (T).

Initially, pressure and temperature inside the vessel are assumed to be constant and equal to $p = 5$ Pa and $T = T_0$. The breach diameter is $d_{\mathrm{breach}} = 10\,\mathrm{cm}$.

The evolution of the gas velocity at different times is shown in Figure 17. It displays how a shock wave is transmitted at the beginning of the pressurization process which is responsible for the mobilization process.

The evolution of the particle concentration has been depicted in Figure 18 at different times.

5. CONCLUSIONS

This paper has dealt with multiphase mixtures of gas and particles. Two different models have been studied, one for dense flows and another for high-dilute mixtures. A finite volume approach for multidimensional problems in unstructured grids has been posed, and several numerical schemes have been extended to analyse this type of mixtures. The AUSM$^+$up scheme has been extended to dense mixtures and in the case of high-dilute mixtures it has only been applied to the gas phase. The Rusanov scheme and a modified version of the AUSM+ have been proposed for the solid phase for high-dilute mixtures. Different numerical benchmarks have shown that the schemes behave quite well in the analysis of problems involving discontinuities. Several shock

DOI: 10.1002/fld

tube problems have been analysed and both the mobilization of a particle layer by a rarefaction wave and the fluidization of a particle bed have been examined and compared with experimental results. In general, the results match qualitatively quite well when comparing with other authors' results. Some discrepancies have been observed between numerical and experimental results in the fluidization test, therefore, perhaps the correlations used to model the physical phenomena taking place in the mixture need further improvements. Despite the fact that most of the tests are numerical tests which originally lack of some specification parameters, they have only provided a good view of the capabilities of the numerical schemes proposed and qualitatively demonstrate their good behaviour in the characterization of discontinuities and their easy adaptability to different flow models. The foregoing work has been carried out in the context of the ITER project. In our opinion, and in order to validate this numerical methods for their use suitably, new experiments must be performed. The authors expect that new experimental data will be available in the near future for this purpose. The addition of more realistic closure laws will also contribute to a more complete model (i.e. turbulence, lift forces, adhesion-entrainment models and so on).

ACKNOWLEDGEMENTS

The authors would like to thank to Ms Juan Mari Belchí and Ms Neasa Conroy for helping them with their English.

REFERENCES

1. Gidaspow D. Hydrodynamics of fluidisation and heat transfer. Supercomputer modeling. *Applied Mechanics Review* 1983; **39**:1–23.
2. Baer MR, Nunziato JW. A two-phase mixture theory for the deflagration-to -detonation transition (DDT) in reactive materials. *International Journal of Multiphase Flow* 1986; **12**:861–889.
3. Bdzil JB, Menikoff R, Son SF, Kapila AK, Stewart DS. Two-phase modelling of deflagration-to-detonation transition in granular materials: a critical examination of modelling issues. *Physics of Fluids* 1999; **11**:378–402.
4. García Cascales JR, Paillère H. Application of AUSM schemes to multi-dimensional compressible two-phase flow problems. *Nuclear Engineering and Design* 2006; **236**:1225–1239.
5. Liou MS. A sequel to AUSM, Part II: AUSM + up for all speeds. *Journal of Computational Physics* 2006; **214**:137–170.
6. Crowe CT, Sommerfeld M, Tsuji Y. *Multiphase Flows With Droplets and Particles*. CRC Press LLC: Boca Raton, FL, U.S.A., 1998.
7. Tsuo YP, Gidaspow D. Computation of flow patterns in circulating fluidized beds. *AIChE Journal* 1990; **36**: 885–896.
8. Harris SE, Crighton DG. Solitons, solitary waves and voidage disturbances in gas-fluidized beds. *Journal of Fluid Mechanics* 1994; **266**:243–276.
9. Combe L, Hérard JM. Un schéma volumes-finis pour la simulation d'un modèle bi-fluide d'écoulements diphasiques compressibles gaz-solide. *Revue Européenne des Éléments Finis* 1997; **6**:197–231.
10. Krispin J, Collins JP. Simulation of dusty flows in an incompressible gas using the projection method. *Twenty-sixth AIAA Fluid Dynamics Conference*, *AIAA 95-2164*, San Diego, CA, U.S.A., 19–22 June 1995.
11. Toro EF. Riemann problem-based techniques for computing reactive two-phase flows. *CoA Report 8815*, Aerodynamics, Cranfield Institute of Technology, 1988.
12. Rogue X, Rodriguez G, Haas JF, Saurel R. Experimental and numerical investigation of the shock-induced fluidization of a particles bed. *Shock Waves* 1998; **8**:29–45.
13. Saurel R, Larini M, Loraud JC. Ignition and growth of a detonation by a high energy plasma. *Shock Waves* 1992; **2**:19–29.
14. Edwards JR, Liou MS. Low-diffusion flux splitting methods for flow at all speeds. *AIAA Journal* 1998; **36**: 1610–1617.
15. Liou, MS. A sequel to AUSM: AUSM+. *Journal of Computational Physics* 1996; **129**:364–382.

DOI: 10.1002/fld

16. Miura H, Glass, II. On dusty-gas shock tube. *Proceeding of the Royal Society of London* 1982; **382**:373–388.
17. Saito T. Numerical analysis of dusty-gas flow. *Journal of Computational Physics* 2002; **176**:129–144.
18. Klemens R, Kosinski P. Numerical simulation of dust layer dispersion due to rarefaction waves. *Eighteenth International Colloquium on the Dynamics of Explosions and Reactive Systems*, Seattle, WA, U.S.A., 2001.
19. Klemens R, Kosinski P, Wolanski P, Korobeinov VP, Markov VV, Menshov IS, Semenov IV. Numerical study of dust lifting in a channel with vertical obstacles. *Journal of Loss Prevention in the Process Industries* 2001; **14**:469–473.
20. Collins JP, Ferguson RE, Chien K, Kuhl AL, Krispin J, Glaz HM. Simulation of shock-induced dusty gas flows using various models. *Twenty-fifth AIAA Fluid Dynamics Conference*, *AIAA 94-2309*, Colorado Springs, U.S.A., 20–23 June 1994.
21. Saurel R, Forestier A, Veyret D, Loraud JC. A finite volume scheme for two-phase compressible flows. *International Journal for Numerical Methods in Fluids* 1994; **18**:803–819.
22. Daniel E, Loraud JC. Numerical simulation of two-phase dilute flow in a diffuser pipe. *International Journal of Numerical Methods for Heat and Fluid Flow* 1998; **8**:224–244.
23. Niu YY. Advection upwinding splitting method to solve a compressible two-fluid model. *International Journal for Numerical Methods in Fluids* 2001; **36**:351–371.
24. Saurel R, Abgrall R. A multiphase Godunov method for compressible multifluid and multiphase flows. *Journal of Computational Physics* 1999; **150**:425–467.
25. Abgrall R, Saurel R. Discrete equations for physical and numerical compressible multiphase mixtures. *Journal of Computational Physics* 2003; **186**:361–396.
26. Rusanov VV. Calculation of interaction of non-steady shock waves with obstacles. *Journal of Computational Mathematics and Physics*, *USSR* 1961; **1**:267–279.
27. Beccantini A, Paillère H. Modelling of hydrogen detonation for application to reactor safety. *Sixth International Conference on Nuclear Engineering*, *Paper ICONE6-6253*, San Diego, CA, U.S.A., May 1998.
28. Paillère, H, Corre C, García Cascales JR. On the extension of the AUSM+ scheme to compressible two-fluid models. *Computers and Fluids* 2003; **32**:891–916.
29. CAST3M website. http://www-cast3m.cea.fr/cast3m/index.jsp
30. Combe L, Hérard JM. Finite volume algorithm to compute dense compressible gas–solid flows. *AIAA Journal* 1999; **37**:337–345.
31. Klemens R, Kosinski P, Oleszczak P. Mathematical modelling of dust layer dispersion due to rarefaction waves. *Archivum Combustionis* 2002; **22**:3–12.
32. Otterman B, Levine A. Analysis of gas–solid particles in shock tubes. *AIAA Journal* 1974; **12**:579–580.
33. Medvedev SP, Geng JH, Grönig H. Shock tube study of dust layer dispersion by rarefaction wave. *Proceedings of the Fifth International Colloquium on Dust Explosions*, Pultusk, 1993.

DOI: 10.1002/fld